Interventional multispectral photoacoustic imaging with a clinical ultrasound probe for discriminating nerves and tendons: an *ex vivo* pilot study

Jean Martial Mari
Wenfeng Xia
Simeon J. West
Adrien E. Desjardins

SPIE.

Interventional multispectral photoacoustic imaging with a clinical ultrasound probe for discriminating nerves and tendons: an *ex vivo* pilot study

Jean Martial Mari,[a,b,†] **Wenfeng Xia,**[a,*,†]
Simeon J. West,[c] **and Adrien E. Desjardins**[a]
[a]University College London, Department of Medical Physics and Biomedical Engineering, Gower Street, London WC1E 6BT, United Kingdom
[b]University of French Polynesia, GePaSud, Faa'a 98702, French Polynesia, France
[c]University College Hospital, Department of Anaesthesia, Main Theatres, Maple Bridge Link Corridor, Podium 3, 235 Euston Road, London NW1 2BU, United Kingdom

Abstract. Accurate and efficient identification of nerves is an essential component of peripheral nerve blocks. While ultrasound (US) imaging is increasingly used as a guidance modality, it often provides insufficient contrast for identifying nerves from surrounding tissues such as tendons. Electrical nerve stimulators can be used in conjunction with US imaging for discriminating nerves from surrounding tissues, but they are insufficient to reliably prevent neural punctures, so that alternative methods are highly desirable. In this study, an interventional multispectral photoacoustic (PA) imaging system was used to directly compare the signal amplitudes and spectra acquired from nerves and tendons *ex vivo*, for the first time. The results indicate that the system can provide significantly higher image contrast for discriminating nerves and tendons than that provided by US imaging. As such, photoacoustic imaging could be valuable as an adjunct to US for guiding peripheral nerve blocks. © 2015 Society of Photo-Optical Instrumentation Engineers (SPIE) [DOI: 10.1117/1.JBO.20.11.110503]

Accurate and efficient identification of nerves is critically important in interventional pain management procedures such as nerve blocks. With nerve blocks, ultrasound (US) imaging is often useful to guide a medical needle for injections of anesthetics. However, with US imaging it can be very challenging to identify nerves, especially when they are within the vicinity of tendons that often have similar appearances.[1,2] More critically, accidental intraneural injections can cause permanent nerve damage.[3]

Several methods have been implemented in clinical practice to facilitate nerve identification.[1] Traditional approaches used paresthesia, in which contact between the nerve and the needle were detected by the patient. Today, nerve stimulators are often used in conjunction with US for discriminating nerves from surrounding tissues. However, there is a poor correlation between the threshold for nerve stimulation and the distance between the needle tip and the nerve, and alternative methods are highly desirable.[4,5]

Optical methods for detecting nerves have attracted increasing interest in recent years.[6–12] Optical reflectance spectroscopy is able to identify spectroscopic tissue signatures and thus was used to guide nerve blocks in swine and human patients.[6–8] Other methods such as confocal imaging,[9] coherent anti-Stokes Raman scattering microscopy,[10] optical coherence tomography,[11] and fluorescence imaging with exogeneous contrast agents[12] have been used. However, all optical imaging modalities suffer from a depth-resolution tradeoff, in which poor spatial resolution is obtained at depths beyond the ballistic region (typically ∼1 mm).

Multispectral photoacoustic (PA) imaging could be a useful modality for visualizing nerves in a clinical setting. It provides rich optical contrast and spectroscopic tissue specificity. Additionally, the spatial resolution can be acoustically defined, so that it is not dependent on achieving a light focus in tissue.[13] It is well known that multispectral PA imaging can identify lipid-rich tissue structures;[14] nerves and atherosclerotic arteries have been imaged with microscopic and wide-field PA using this principle.[15–17] In the Li et al. study,[16] a clinical US imaging probe was used for reception with surface-based illumination. This type of illumination may be well suited to superficial nerves, but visualization of deeper nerves could be challenging due to the rapid reduction of PA sensitivity with increasing imaging depth. Interventional PA imaging addresses this issue by delivering light inside the body, and detecting US at the tissue surface.[18–23]

An interventional multispectral PA (IMPA) imaging system was developed in the authors' group.[21–23] The system was characterized in previous studies using phantoms and fatty tissues.[21,22] In this study, an IMPA system was used to directly compare PA signal amplitudes and spectra acquired from excised nerves and tendons. To the authors' knowledge, this comparison had not previously been made.

The IMPA system (Fig. 1) was based on a clinical US imaging system (Ultravision, Winprobe, Florida) with excitation light provided by an optical parametric oscillator (OPO, VersaScan L-532, VersaScan L-532, GWU-Lasertechnik, Erftstadt, Germany), pumped by a Nd:YAG laser (repetition rate: 10 Hz; pulse width: 6 to 9 ns; Quanta-Ray, INDI-40-10, Spectra-Physics, Santa Clara, California). The idler beam of the OPO, with a tunable wavelength range of 1100 to 2200 nm, was coupled to an optical fiber with silica-core/silica-cladding and a core diameter of 910 μm. US reception was performed with a clinical linear array US imaging probe (L14-5/38), with a nominal bandwidth and geometric focus of 5 to 14 MHz and 16 mm, respectively. Acquisition of PA
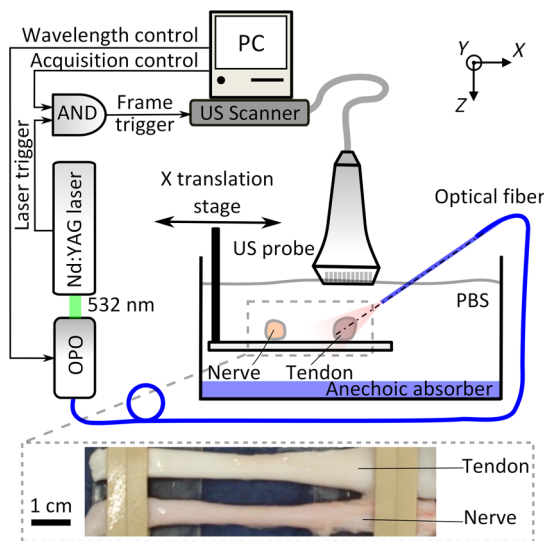
Fig. 1 (Top) Schematic of the interventional multispectral photoacoustic (PA) imaging system. (Bottom) Photograph of a nerve and tendon pair, affixed by rubber bands.

images was triggered by the synchronization signals of the OPO (Fig. 1). Since the OPO light pulses occurred at the constant rate of 10 Hz, a logic AND gate was used to control triggering of the US system and thereby to provide control over the image acquisition speed. PA images were reconstructed online using a backprojection algorithm. A standard US B-mode image was acquired immediately after each PA image acquisition, with postbeam formed radio frequency data sampled at 40 MHz. PA and US images were transferred to a personal computer for postprocessing.

Four nerves and tendons from the brachial plexus and from the upper foot, respectively, were excised from two swine immediately postmortem at the Northwick Park Institute for Medical Research (London, United Kingdom). For US and PA imaging, a nerve and a tendon were affixed in parallel on a translation stage, in a tank filled with phosphate-buffered saline (PBS) solution at the room temperature (Fig. 1). The nerve and tendon (each approximately 10 cm in length) were positioned perpendicular to the imaging plane at the same depth. The light delivery fiber was inserted in-plane so that its tip position could be identified on the US image. Excitation light from this fiber was largely unscattered by the PBS; it was first directed only at the tendon (Fig. 1), and then it was directed only at the nerve after the nerve/tendon pair was laterally translated. The position of the light delivery fiber was constant. Each multispectral PA image sequence comprised 21 acquisitions, which were performed at light wavelengths that varied from 1160 to 1260 nm in steps of 5 nm. At each wavelength, 25 repeated images were acquired. While the energy per pulse was approximately constant at each wavelength (7 mJ), the pulse energies at each wavelength were used to normalize the acquired PA image frames. The light fluence at the tissue surface was below the ANSI limit for exposure to skin (100 mJ/cm^2).[24] The fluence was estimated without accounting for the light absorption in the water path; the actual fluence on the tissue surface was even lower than our estimation. With the first three nerve/tendon pairs, imaging was performed at a single location along the tissue axis; the fourth pair was longer in length and allowed for imaging at three nonoverlapping locations.

To calculate PA spectra from a region of interest (ROI), PA amplitudes were averaged across the ROI and over repeated images. Normalized PA spectra were used to perform averaging across multiple samples. For normalization, the first step was to average the noise-subtracted PA spectrum across measured wavelengths. As the second step, a normalization factor was calculated so that this average was equal for all nerve samples. The third step was to apply this normalization factor as a multiplicative term to PA spectra from both nerve and tendon samples.

Images acquired from a representative nerve/tendon pair are shown in Fig. 2. The US and PA images had a good spatial correspondence. In the US images, the nerves and tendons had similar visual appearances [Figs. 2(a) and 2(b)]. With PA imaging, the two tissues presented very differently. When excitation light was directed only to tendons, very small PA signals were observed [Fig. 2(c)]. When excitation light was directed only to nerves, the surface and part of the interior of the nerves were clearly apparent at wavelengths in the vicinity of 1210 nm [Fig. 2(d)]. The mean PA spectrum obtained from an ROI enclosing the first nerve corresponded well to the optical absorption spectrum of lipid [Fig. 2(e)]. The mean normalized PA spectrum obtained from this same ROI was very similar to that of the mean PA spectrum obtained from the first nerve and it had comparable standard deviations [Fig. 2(f)].

To compare how nerves and tendons can be differentiated with PA and US imaging, the image contrast corresponding to each of these two modalities was calculated as follows:

$$\text{Contrast} = \frac{|\bar{S}_{\text{Nerve}} - \bar{S}_{\text{Tendon}}|}{|\bar{S}_{\text{Nerve}} + \bar{S}_{\text{Tendon}}|}, \tag{1}$$

where $\bar{S}_{\text{Nerve}}$ and $\bar{S}_{\text{Tendon}}$ are the signal amplitudes averaged over ROIs surrounding these respective tissues. For PA images, contrast was calculated after averaging across acquisitions performed with the excitation light wavelengths of 1205, 1210, and 1215 nm. A comparison between the contrast from PA and US was made using a paired t-test, with the assumption that all six sample pairs were independent. As shown in Fig. 3, the estimated PA contrast was significantly higher than the US contrast ($p < 0.05$).

In this study, the excitation light was delivered through an optical fiber to the ROI. This configuration could be beneficial for imaging nerve structures that are beyond the imaging depth of PA imaging systems with surface-based excitation light delivery. Follow-on *in vivo* studies and simulations are required to determine under what conditions through-needle delivery is preferable to surface-based delivery, and to determine how the presence of optical scattering and absorption between the optical fiber and the tissue target affects PA signal amplitudes and spectra.

The results of this study suggest that lipids could be a useful source of endogenous contrast for differentiating nerves from tendons with multispectral PA imaging. Within nerves, lipids are known to be present within myelin sheaths and in intraneural adipose tissue. However, care will be needed to interpret PA images obtained *in vivo*, as lipids are also found in several other locations, such as perineural adipose tissue and fascial planes. If a tissue structure is known to be either a nerve or a tendon, PA contrast is likely to be useful for differentiating the two-tissue structures. However, determining whether an arbitrary lipid-rich structure in tissue corresponds to a nerve is a different problem. US imaging could be beneficial in terms of providing
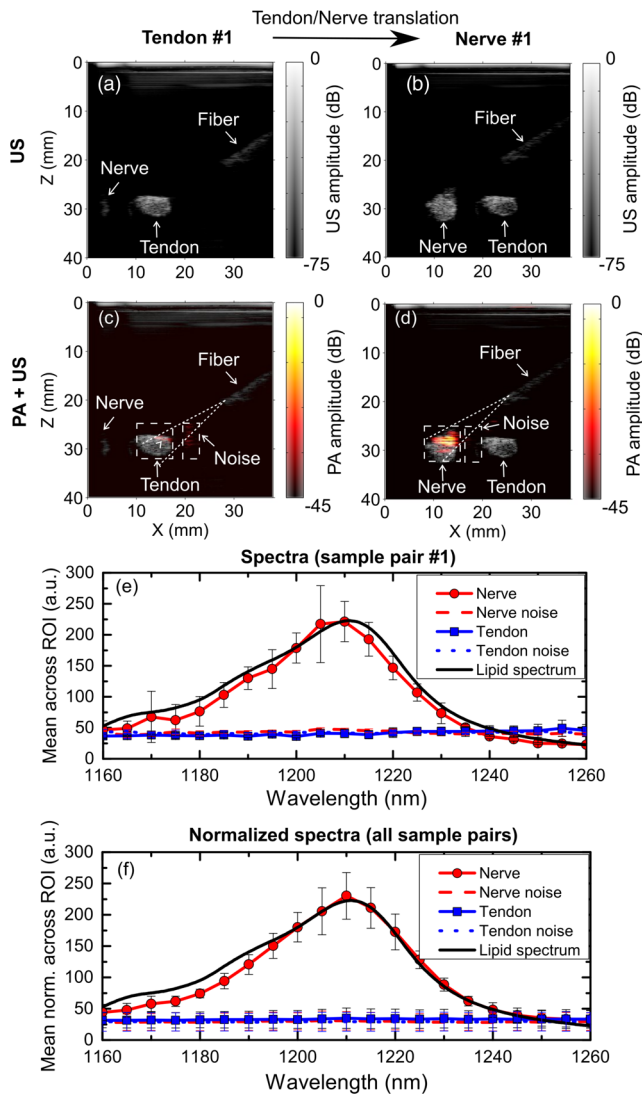
Fig. 2 Interventional multispectral PA imaging and US imaging of a nerve/tendon pair. US images of the tendon and nerve samples (pair #1) are shown in (a) and (b), respectively. PA images of this nerve/tendon pair are superimposed on the corresponding US images in (c) and (d). A small PA signal from the tendon is indicated with a "V" in (c). The dashed lines are marginal rays that indicate the angular range of light emerging from the fiber. The images (c) and (d) were normalized to the maximum value of image (d), and they are displayed on the same color scale. PA amplitudes acquired from nerve/tendon pair #1, which were averaged over regions of interest (ROIs) [dashed boxes in (c), (d)] and over the repeated images, are shown in (e). The optical absorption spectrum of lipid, obtained from Ref. 25 and scaled relative to the maximum value of the nerve spectrum, is provided for comparison. Normalized PA amplitudes acquired from all sample pairs, which were averaged over ROIs, over repeated images, and across samples, are shown in (f). The error bars in (e) and (f) are standard deviations that were calculated from the 25 repeated images and from the six samples, respectively. The normalization procedure is described in the text.

Fig. 3 Photoacoustic and ultrasound image contrast calculated from six measurements, acquired from four nerve and tendon pairs. Error bars represent the standard deviations. *$p < 0.05$.

With *in vivo* imaging, nerves and tendons will present differently than they did in this study, as they are surrounded by multiple types of optically heterogeneous tissues. As a result, both scattering and absorption in the background will likely be more prominent; the latter could include contributions from hemoglobin[28] and myoglobin. Spectral unmixing and acquisitions from different wavelength ranges, where hemoglobin and myoglobin absorb more prominently, could, therefore, be valuable to improve contrast for lipids for *in vivo* nerve delineation. In this study, optical scattering and absorption within nerves and tendons were likely responsible for the apparent lack of signals in deeper regions within these tissue structures.

To assist with the guidance of nerve blocks, multispectral PA imaging could be valuable to test hypotheses about the identities of particular tissue structures that are identified with US imaging. In addition to the identifying nerves, PA imaging could also highlight blood vessels to prevent accidental punctures using excitation light with wavelength ranges where hemoglobin absorption is prominent. This study demonstrated that IMPA imaging could be a valuable adjunct modality to US imaging for guiding nerve blocks, as it has the potential to decrease complication rates and improve procedural efficiency.

anatomical information. With through-needle delivery of excitation light, there is the potential for optical stimulation,[26,27] which could serve as an additional method for identifying nerves. Ultimately, the sensitivity and specificity with which nerves can be identified will depend on the particular comparison that is made, and additional information that is available.
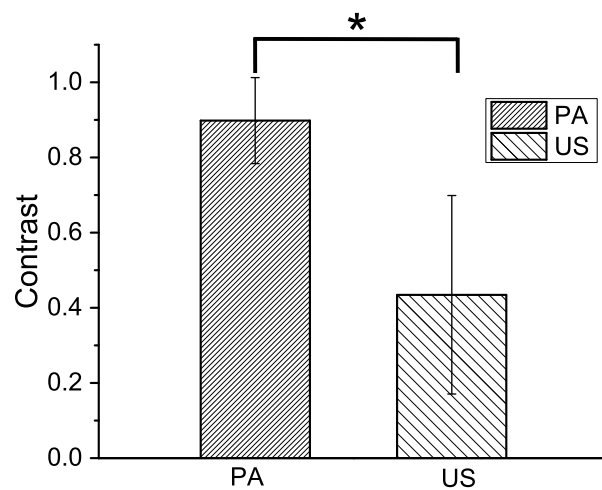
References

1. L. Helen, B. D. O'Donnell, and E. Moore, "Nerve localization techniques for peripheral nerve block and possible future directions," *Acta Anaesthesiol. Scand.* **59**(8), 962–974 (2015).
2. D. A. Jamadar et al., "Musculoskeletal sonography: important imaging pitfalls," *Am. J. Roentgenol.* **194**(1), 216–225 (2010).
3. C. L. Jeng, T. M. Torrillo, and M. A. Rosenblatt, "Complications of peripheral nerve blocks," *Br. J. Anaesth.* **105**(Suppl. 1), i97–i107 (2010).

4. P. E. Bigeleisen, N. Moayeri, and G. J. Groen, "Extraneural versus intra-neural stimulation thresholds during ultrasound-guided supraclavicular block," *Anesthesiology* **110**(6), 1235–1243 (2009).

5. M. L. Beach, B. D. Sites, and J. D. Gallagher, "Use of a nerve stimulator does not improve the efficacy of ultrasound-guided supraclavicular nerve blocks," *J. Clin. Anesth.* **18**(8), 580–584 (2006).

6. M. Brynolf et al., "Optical detection of the brachial plexus for peripheral nerve blocks," *Reg. Anesth. Pain Med.* **36**(4), 350–357 (2011).

7. A. E. Desjardins et al., "Needle stylet with integrated optical fibers for spectroscopic contrast during peripheral nerve blocks," *J. Biomed. Opt.* **16**(7), 077004 (2011).

8. A. Balthasar et al., "Optical detection of peripheral nerves: an in vivo human study," *Reg. Anesth. Pain Med.* **37**(3), 277–282 (2012).

9. Y. Wu et al., "Confocal imaging reveals three-dimensional fine structure difference between ventral and dorsal nerve roots," *J. Biomed. Opt.* **16**(5), 050502 (2011).

10. L. Gao et al., "Label-free high-resolution imaging of prostate glands and cavernous nerves using coherent anti-Stokes Raman scattering micros-copy," *Biomed. Opt. Express* **2**(4), 915–926 (2011).

11. D. T. Raphael et al., "Images of spinal nerves and adjacent structures with optical coherence tomography: preliminary animal studies," *J. Pain* **8**(10), 767–773 (2007).

12. M. A. Whitney et al., "Fluorescent peptides highlight peripheral nerves during surgery in mice," *Nat. Biotechnol.* **29**(4), 352–356 (2011).

13. P. C. Beard, "Biomedical photoacoustic imaging," *Interface Focus* **1**(4), 602–631 (2011).

14. T. J. Allen et al., "Spectroscopic photoacoustic imaging of lipid-rich plaques in the human aorta in the 740 to 1400 nm wavelength range," *J. Biomed. Opt.* **17**(6), 061209 (2012).

15. T. P. Matthews et al., "Label-free photoacoustic microscopy of periph-eral nerves," *J. Biomed. Opt.* **19**(1), 016004 (2014).

16. R. Li et al., "Label-free *in vivo* imaging of peripheral nerve by multi-spectral photoacoustic tomography," *J. Biophotonics*, 1–5 (2015).

17. K. Jansen et al., "Intravascular photoacoustic imaging of human coro-nary atherosclerosis," *Opt. Lett.* **36**(5), 597–599 (2011).

18. D. Piras et al., "Photoacoustic needle: minimally invasive guidance to biopsy," *J. Biomed. Opt.* **18**(7), 070502 (2013).

19. M. A. Lediju Bell et al., "Localization of transcranial targets for photo-acoustic-guided endonasal surgeries," *Photoacoustics* **3**(2), 78–87 (2015).

20. L. Lin et al., "In vivo deep brain imaging of rats using oral-cavity illu-minated photoacoustic computed tomography," *J. Biomed. Opt.* **20**(1), 016019 (2015).

21. W. Xia et al., "Performance characteristics of an interventional multi-spectral photoacoustic imaging system for guiding minimally invasive procedures," *J. Biomed. Opt.* **20**(8), 086005 (2015).

22. W. Xia et al., "An interventional multispectral photoacoustic imaging platform for the guidance of minimally invasive procedures," *Proc. SPIE* **9539**, 95390D (2015).

23. W. Xia et al., "Interventional photoacoustic imaging of the human pla-centa with ultrasonic tracking for minimally invasive fetal surgeries," *Lect. Notes Comput. Sci.* **9349**, 371–378 (2015).

24. Laser Institute of America, "American national standard for safe use of lasers," ANSI Z136.1-2007, American National Standards Institute, Inc. (2007).

25. R. Nachabe et al., "Estimation of biological chromophores using diffuse optical spectroscopy: benefit of extending the UV-VIS wavelength range to include 1000 to 1600 nm," *Biomed. Opt. Express* **1**(5), 1432–1442 (2010).

26. J. Wells et al., "Biophysical mechanisms of transient optical stimulation of peripheral nerve," *Biophys. J.* **93**(7), 2567–2580 (2007).

27. J. Wells et al., "Optical stimulation of neural tissue in vivo," *Opt. Lett.* **30**(5), 504–506 (2005).

28. P. Wang, "In vivo photoacoustic micro-imaging of microvascular changes for Achilles tendon injury on a mouse model," *Biomed. Opt. Express* **2**(6), 1462–1469 (2011).